AGU PUBLICATIONS

Water Resources Research

RESEARCH ARTICLE
10.1002/2015WR017062

Key Points:
- Multicentennial December–January hydrological reconstructions western Tasmania
- Twentieth century wetter than average, severe extended dry periods in past
- Nontraditional tree ring chronologies key to successful reconstructions

Supporting Information:
- Supporting Information S1

Correspondence to:
K. J. Allen,
Kathryn.Allen@unimelb.edu.au

Citation:
Allen, K. J., S. C. Nichols, R. Evans, E. R. Cook, S. Allie, G. Carson, F. Ling, and P. J. Baker (2015), Preliminary December–January inflow and streamflow reconstructions from tree rings for western Tasmania, southeastern Australia, *Water Resour. Res.*, *51*, doi:10.1002/2015WR017062.

Received 6 FEB 2015
Accepted 9 JUN 2015
Accepted article online 15 JUN 2015

Preliminary December–January inflow and streamflow reconstructions from tree rings for western Tasmania, southeastern Australia

K. J. Allen[1], S. C. Nichols[1], R. Evans[2], E. R. Cook[3], S. Allie[4], G. Carson[4], F. Ling[5], and P. J. Baker[1]

[1]Department of Ecosystem and Forest Science, University of Melbourne, Richmond, Victoria, Australia, [2]Silviscan Pty Ltd, Melbourne, Victoria, Australia, [3]Lamont-Doherty Earth Observatory, Palisades, New York, USA, [4]Hydro Tasmania, Hobart, Tasmania, Australia, [5]Entura Consulting, Hydro Tasmania, Cambridge, Tasmania, Australia

Abstract Projected decreases and changes in the seasonal distribution of precipitation will have profound impacts on southeastern Australia, including its ability to generate renewable hydroelectricity. Recent decreases in precipitation over the region may be significant in the context of instrumental records, but the question of whether these decreases are within long-term natural variability remains. To help address this issue, we present December–January streamflow and dam inflow reconstructions for southeastern Australia. These reconstructions for the Tasmanian west coast are based solely on local tree ring chronologies and span up to 1600 years. Nonparametric estimates, however, indicate good model skill for the last 458 years (streamflow) and 478 years (dam inflow). The reconstructions indicate that twentieth century conditions were well within the range of historical variability, and were in fact relatively wet. The period from approximately 1600 to 1750 CE was one of the enhanced variability and a high proportion of low and high flow events occurred in the seventeenth century. There are significant relationships between streamflow and inflow reconstructions and large-scale ocean-atmosphere processes such as ENSO and the Southern Annular Mode. Critically, our two reconstructions rely heavily on new tree ring chronologies based on properties such as tracheid radial diameter, cell wall thickness, and density, underscoring the importance of these different types of chronologies in reconstructions.

1. Introduction

Hydrological conditions have been linked to the rise and fall of major civilizations around the world [*Buckley et al.*, 2010; *Stahle et al.*, 2011; *Marshall*, 2012; *Pederson et al.*, 2014] and help define the geographical distribution of major human settlements. The southeastern region of Australia (SEA) is the most densely populated part of the Australian continent and supports extensive agricultural activity. The devastating impacts of major droughts on SEA are well known [*Van Dijk et al.*, 2013] and the most recent of these, the Big Dry (~1997–2009), has intensified the focus on predicting water resources for the region into the future. A general decline in precipitation in SEA over the past 40 years has also been widely observed [e.g., *Cai and Cowan*, 2008; *Cai et al.*, 2009; *Murphy and Timbal*, 2008; *Bennett et al.*, 2010; *Hope et al.*, 2010; *Chiew et al.*, 2011], prompting concerns that the region is experiencing a departure from historical conditions [*Chiew et al.*, 2011]. Over the past 20 years in particular, this decline has negatively impacted urban water supplies, agricultural food production, river discharge required to sustain the aquatic environment, and capacity to generate hydroelectricity. To make matters worse, various modeling studies indicate that drying of southern southeastern Australia is likely to increase over the course of the 21st century [*CSIRO*, 2008; *Timbal and Jones*, 2008; *Viney et al.*, 2009; *Chiew et al.*, 2011, 2014; *Post et al.*, 2014]. Predictions also suggest that the seasonal distribution of precipitation across the region is expected to change [*Bennett et al.*, 2010; *Chiew et al.*, 2011]. Current declines in available water resources and changes in the seasonal distribution of precipitation pose considerable challenges for SEA's renewable hydroelectricity sector. The region produces the majority of Australia's hydroelectricity, with Tasmania in the far southeast being responsible for approximately 60% of its generation capacity. Like the rest of SEA, Tasmania has experienced declining precipitation since the mid-1970s, with greatest decreases occurring in the autumn months, and in the north and east of the state [*Grose et al.*, 2010]. Since 1975, there has been a decrease in the number of very wet years, although

Taschetto and England [2008] note an increase in winter and spring precipitation in the west. Such changes affect decisions concerning storage levels in Tasmanian impoundments that are made on the basis of detailed climate projections and resource modeling within the existing, and shifting, Australian energy policy nexus.

Analyses of observed data and models of future change are inherently constrained by limited variability present in relatively short ($\leq$100 years) meteorological records. *Post* [2013], for example, acknowledged difficulties in applying hydrological models to conditions in which modeled precipitation differs from historical precipitation by more than 15%. There is, therefore, a particular need for very long records that incorporate a greater range of hydrological conditions than is available from the existing meteorological records [cf. *Chiew et al*., 2014]. Paleohydrological reconstructions have enabled water managers to put 20th and 21st century conditions in the context of much longer records [*Sheppard et al*., 2004; *Touchan et al*., 2011; *Cook et al*., 2010; *Wilson et al*., 2005; *Urrutia et al*., 2011]. Many of these paleohydrological records indicate that conditions much more challenging than those of the past 100 years have existed in the past, and for much more extended periods [*Treydte et al*., 2006; *Stahle et al*., 2007; *Buckley et al*., 2010; *Chen et al*., 2012]. Despite the increasingly urgent need to better understand long-term hydrological dynamics in SEA against the backdrop of rapid climate change [*Van Dijk et al*., 2013], there is a paucity of high-resolution paleohydrological reconstructions for the region primarily due to the lack of suitable hydrological proxies. Thus far, the only attempts at developing annual-resolution hydrological reconstructions for the region have relied on records that are mostly outside the SEA region [*McGowan et al*., 2009; *Gergis et al*., 2011; *Gallant and Gergis*, 2011].

Not only does Tasmania supply approximately 60% of Australia's hydroelectricity, it also boasts an impressive number of multicentennial annually dated tree ring width chronologies [*Heinrich and Allen*, 2013]. This stands in stark contrast to mainland Australia where, due to species-related limitations, very few published chronologies extend back for more than 200 years [e.g., *Cullen and Grierson*, 2009]. Thus far, the majority of the Tasmanian ring width chronologies have shown stronger, albeit often complex, relationships with regional temperature than with hydroclimate [*Buckley et al*., 1997; *Allen et al*., 2001, 2011]. Recent work, however, indicates that tree ring chronologies based on properties such as tracheid radial diameter, microfibril angle, density, and cell wall thickness are likely to play an important role in the development of seasonal paleohydrological reconstructions from the mesic Tasmanian species [*Drew et al*., 2013; K. J. Allen et al., 2015, Palaeohydrology in climatological context: Seasonal characteristics of streamflow in part of southeastern Australia, submitted to *Applied Geography*]. Here we present the first December–January reconstructions of a streamflow index for the central west of Tasmania, and of inflows to the Lake Burbury impoundment, also in the central west of Tasmania. Critically, due to ocean-atmosphere-topography interactions that determine the climate of this part of southeastern Australia, we are able to rely exclusively on local tree ring predictors for these reconstructions. Although there is a pronounced seasonal cycle in western Tasmanian precipitation (and hence streamflows) with a peak in the winter and spring months (www.bom.gov.au), December–January (DJ) streamflows and subsequent inflows to impoundments are important to hydroelectricity generators because they provide a buffer against delayed autumn-winter rains. Indeed, delays in autumn-winter rains have become more common in recent years [*Murphy and Timbal*, 2008; *Pook et al*., 2006]. This results in the need to import coal-fire generated electricity from mainland Australia into Tasmania rather than the ability to export hydroelectricity. It also increases the cost of electricity to end-users. Conversely, wet summers provide water managers with some flexibility if autumn-winter rains are delayed. Therefore, a paleohydrological record of summer conditions in western Tasmania will provide water managers with much needed longer-term information about summer flow variability that can be incorporated into water availability models.

2. Methods

2.1. The Study Region and Drivers of Local Precipitation

The island state of Tasmania is located in the far southeast of Australia (Figure 1). There are few population centers in the rugged western portion of Tasmania, and none in the remote southwest. A strong rainfall gradient across the state results in approximately 2000–3000 mm of rain falling annually in the west of the state but only 500–600 mm typically falling in the east. This rain shadow effect is observable for all seasons,

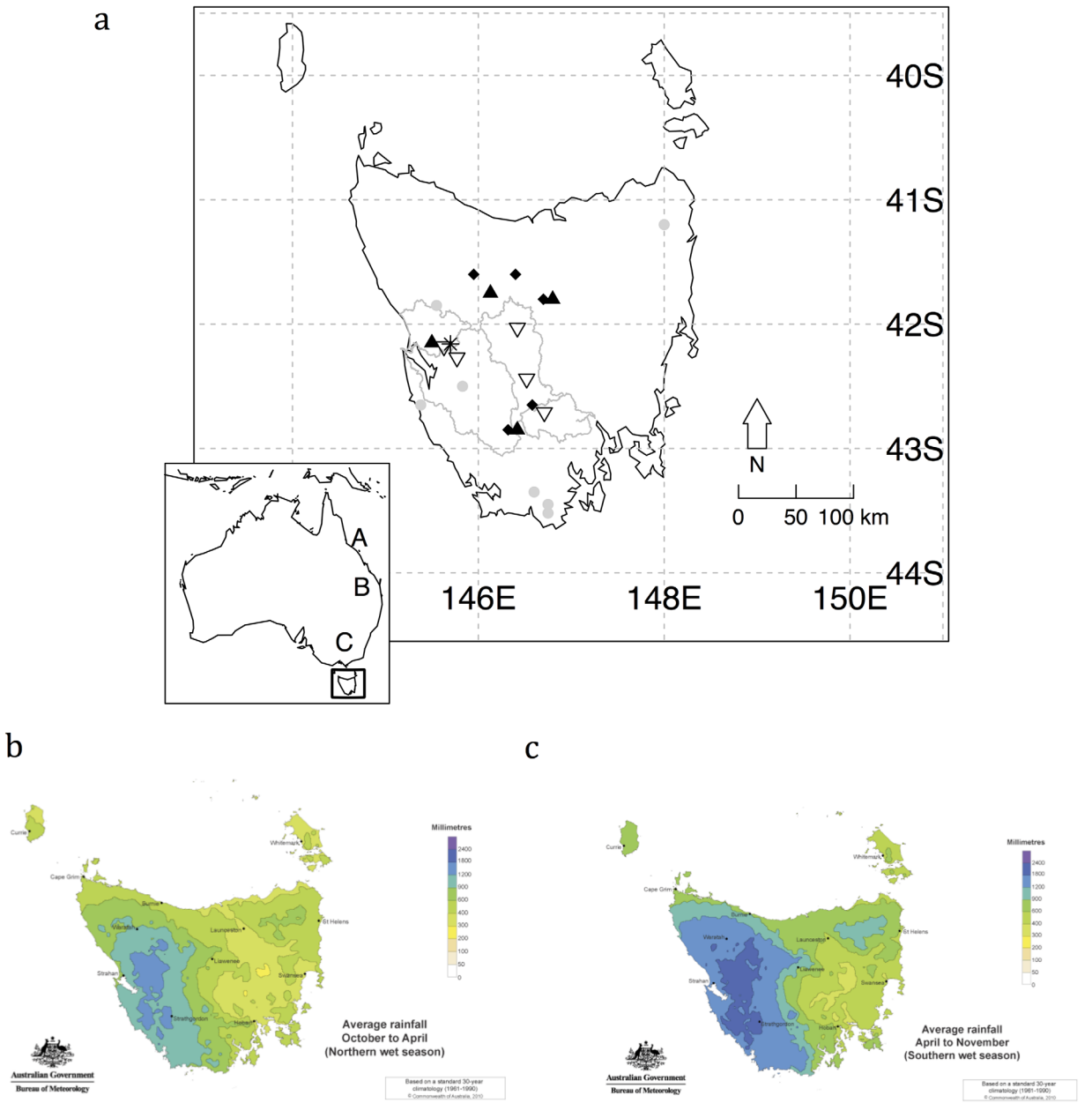

Figure 1. (a) Location of tree ring sites used for reconstructions (solid diamond, tree ring width chronology; solid triangle, wood properties tree ring chronologies), streamflow stations (nabla), and Lake Burbury (asterisk). Solid circle shows location of potential predictors (tree ring sites) that did not meet criterion. All unselected sites were ring width sites. In the inset map of Australia, A shows the location of the Havannah coral record; B is the area in which precipitation is most strongly related to *Vance et al.*'s [2014] IPO positive phases; C represents the Murray Darling Basin for which *Gallant and Gergis* [2011] and *McGowan et al.* [2009] reconstructed streamflow. Distribution of (b) warm and (c) cool season precipitation across Tasmania. Figures sourced from the Bureau of Meteorology (www.bom.gov.au).

but is strongest in the cold season (Figures 1b and 1c). Analysis of catchment flow records across the state indicates the east-west differences among catchments persist for all seasons (Allen et al., submitted manuscript).

Large-scale ocean-atmosphere processes impact on seasonal water availability in the SEA region generally, and also Tasmania specifically [*Cai and Cowan*, 2008; *Risbey et al*., 2009; *Pook et al*., 2006; *Ummenhofer et al*., 2009; *Timbal and Drosdowsky*, 2012; *Post et al*., 2014, among many others]. Typical seasonal and regional signatures of these processes vary, as described by *Risbey et al*. [2009] and summarized for Tasmania by *Grose et al*. [2010]. In brief, the Indian Ocean Dipole (IOD), reflecting sea surface temperature differences in the east and west Indian Ocean, has its strongest influence on Tasmanian precipitation in spring in the north

and east of the state [*Risbey et al*., 2009]. The Southern Oscillation Index (SOI), an indicator for El Niño-Southern Oscillation, is the normalized pressure difference between Taihiti and Darwin, and is most strongly related to southeast Australian precipitation in winter and spring [*Risbey et al*., 2009]. The Interdecadal Pacific Oscillation (IPO) modulates the hydroclimate of southeastern Australia [*Kiem and Verdon-Kidd*, 2009; *Vance et al*., 2014]. Atmospheric blocking predominantly affects precipitation in the Tasmanian east and southwest from autumn to spring [*Pook et al*., 2006]. The dominant influence of the Southern Annular Mode (SAM) on precipitation occurs in western Tasmania for the winter-summer seasons. For western and south-western Tasmania, *Risbey et al*. [2009] single out SAM as the dominant process affecting precipitation in the summer months. The intensification of the subtropical ridge (STR) has also been linked to recent declines in precipitation over SEA generally [*Timbal and Drosdowsky*, 2012; *Post et al*., 2014].

2.2. Tree Ring Chronologies

Although the diversity of Tasmanian river discharge characteristics reflects the geographical and seasonal distribution of precipitation [*Risbey et al*., 2009; *Bennett et al*., 2010; *Grose et al*., 2010], we did not impose expectations related to these geographical and seasonal gradients on the selection of chronologies to be used for the reconstruction. For example, we might expect that chronologies from the north and east of the state would not sufficiently reflect streamflow (inflow) in the west. But this is an assumption that needs to be tested. Thus, we included all Tasmanian tree ring chronologies that spanned at least the AD1800 to 2007 period in our initial pool of 25 chronologies (Figure 1). This multispecies network included *Lagarostrobos franklinii*, *Athrotaxis selaginoides*, *Athrotaxis cupressoides*, and *Phyllocladus aspleniifolius*. Details concerning most of the ring width chronologies can be found elsewhere [*Buckley et al*., 1997; *Allen et al*., 2001, 2011]. Chronologies based on density, cell wall thickness, tracheid radial diameter, and microfibril angle for *Athrotaxis cupressoides*, *Athrotaxis selaginoides*, *Phyllocladus aspleniifolius*, and *Lagarostrobos franklinii* were developed through the use of Silviscan© as described by *Drew et al*. [2013]. Standardization of tree ring series is common practice and aims to remove biological variability present in the individual series thought unrelated to climate [*Cook and Kariukstis*, 1990]. In order to minimize any trend distortion [cf. *Melvin and Briffa*, 2008], each of the five types of series were standardized differently. Raw density series commonly showed a decreasing trend with age and so were standardized with a negative exponential/negative sloping regression line. Due to the lack of decrease or increase of tracheid radial diameter over the life of trees across sites, and the role stand dynamics is likely to have played in at least two of the three sites for which tracheid radial diameter chronologies were produced, tracheid radial diameter series were standardized using the Friedman variable span smoother [*Friedman*, 1984]. The same standardization was applied to the microfibril angle series for the same reason. Cell wall thickness series were standardized with a negative exponential/regression line of any slope due to a commonly observed, but not ubiquitous, increasing trend in raw series. An age-dependent smoothing spline [*Melvin et al*., 2007] was used to standardize ring width chronologies. All chronologies were standardized within the signal-free framework [*Melvin and Briffa*, 2008] and calculated using residuals rather than ratios [*Cook and Peters*, 1997]. Signal-free standardization aims to better preserve common medium frequency variation due to climate that can be lost using nonsignal-free detrending methods. It is based on the premise that the common forcing signal in the tree ring data due to climate can bias the fitting of growth curves used to remove nonclimatic variance and thus lead to a loss of medium frequency signals attributable to climate. Signal-free standardization also eliminates trend distortion effects caused by that same common variability at the ends of series [*Melvin and Briffa*, 2008].

2.3. Streamflow and Inflow Data

Streamflow data from "unimpaired" catchments [*Peel et al*., 2000] in western Tasmania were sourced from Hydro Tasmania and the Department of Primary Industry, Parks, Water, and Environment. "Unimpaired" is defined as streamflow not subject to diversion or regulation. Western Tasmanian streamflows are highly correlated among catchments, but very few series extend back before 1960 and up to the current day (Allen et al., submitted manuscript), which therefore limits the series lengths available for model calibration and verification. In order to extend the length of the series available for calibration and verification purposes, we created a regional index of streamflow for western Tasmania. Highly correlated catchment flows across the region makes this feasible (Allen et al., submitted manuscript). For each streamflow series used, the December and January streamflows were added together and then converted to z-scores. A regional index of streamflow (1946–2007; see below) for western Tasmania was then obtained by averaging these z-scores across all series for each year. Basic information on the selected streamflow series is shown in Table 1 and

Table 1. Characteristics of Streamflow Data Used to Produce the Index of Streamflow and of the Inflow Data for the Burbury Impoundment[a]

River	Period of Record	% Missing Data	Approximate Catchment Size (km^2)
King (78)	Jan 1924 to Dec 1990	0	449
Nive (497)	Jun 1964 to Mar 2013	0	186
Franklin (145)	May 1953 to Mar 2013	1.98	764
Tyenna (449)	Apr 1965 to Mar 2013	1.77	184
Florentine (40)	Feb 1952 to Mar 2013	0	436
Inflow Station			
Burbury inflow	Jan 1924 – Dec 2011	0	556

[a]Numbers in parentheses are Hydro Tasmania gauge numbers. Note that King River flow data prior to 1946 are noted as "low quality" and have not been used in reconstructions here.

Figure 1. Streamflow series from the east and north of the state are not closely related to western streamflow (Allen et al., submitted manuscript) and were therefore not included in the index series.

The larger proportion of precipitation in western Tasmania falls in winter-spring although catchment flows are significant all year round. Numerous impoundments in the area are used to generate hydroelectricity for SEA, and the best quality data available for any of these comes from Lake Burbury, located in Tasmania's central west. These data were provided by Hydro Tasmania. The Lake Burbury impoundment was commissioned in 1991; however, the flows into the basin have been directly measured since 1924 via the streamflow gauge on the King River until 1990. Since 1991, measurement of lake inflow has been based on observed lake levels and power station releases. As for precipitation, inflows are greatest in the winter-spring months although there is considerable variability for all months (Figure 2a). Original flow records for the King River indicate that the first 21 years of the record (1924–1945) is low quality. We therefore excluded both streamflow and inflow data prior to 1946 from our model calibration and verification procedures. A comparison of Burbury inflow and the streamflow index (Figure 2b) illustrates a close relationship between the two series since 1946. Streamflow gauges are all within 105 km of the Burbury impoundment. December–January streamflow patterns do not reflect annual streamflow patterns (e.g., correlations between the King River DJ flows and annual flow were $R = -0.21$ (July–June year) and $R = -0.07$ (October–September year)). The same is true for inflow ($R = -0.03$ (July–June year); $R = -0.01$ (October–September year)). These poor relationships between DJ and annual flows are most likely attributable to highly seasonal effects of different ocean-atmosphere processes on precipitation and streamflow in southeastern Australia. This means that our DJ reconstructions cannot be extrapolated to reflect annual inflows or streamflows.

We have chosen to reconstruct both the streamflow index and Lake Burbury inflows because in theory they should reflect the same general hydroclimate. If the two reconstructions differ greatly from one another, this would decrease confidence in the reconstructions. Conversely, if they are very similar to one another, this enhances confidence in the reconstructions.

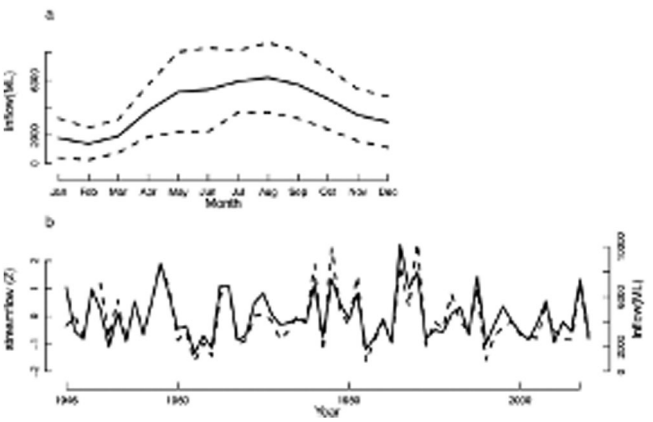

Figure 2. (a) Average monthly inflows, 1946–2011, Lake Burbury. Dotted lines denote 1σ. (b) Comparison of Lake Burbury inflow data and the constructed streamflow index, 1946–2011. Streamflow index is expressed as z-scores.

2.4. Reconstructions

We used a nested point-by-point regression (PPR) technique [*Cook et al.*, 2013] to reconstruct the DJ inflows at Lake Burbury and the regional streamflow index. This technique has been extensively used to develop tree ring based reconstructions elsewhere [e.g., *Cook et al.*, 2010; *Touchan et al.*, 2011; *Pederson et al.*, 2013], and further detail about the basic technique can be found in *Cook et al.* [1999]. The nested approach explicitly acknowledges that the number of predictors typically declines as one goes back in time. Multiple reconstructions are produced, with each successively longer one based on fewer predictors in

Table 2. Tree Ring Chronologies Used in Reconstructions[a]

Chronology	Lat	Long	Species	Full Chronology Length	Lag	Recon	Corr	Beta
Mickey Creek average cell wall thickness	−41.48	146.42	*A. cupressoides*	1354–2009	0	1,2	0.413 0.412	0.246 (9.20) 0.369 (14.4)
Mickey Creek average density	−41.48	146.42	*A. cupressoides*	1354–2009	0	1,2	0.392 0.392	0.210 (7.86) 0.326 (12.7)
February Creek average cell wall thickness	−41.45	146.15	*A. selaginoides*	1583–2011	1	1,2	−0.376 −0.301	−0.190 (7.11) −0.171 (6.67)
February Creek average density	−41.45	146.15	*A. selaginoides*	1583–2011	1	1	−0.288	−0.145 (5.42)
February Creek average tracheid radial diameter	−41.45	146.15	*A. selaginoides*	1599–2011	0	1,2	−0.325 −0.299	−0.112 (4.19) −0.152 (5.92)
TNE average cell wall thickness	−42.2*	146.33	*P. aspleniifolius*	1657–2012	0	1,2	0.432 0.360	0.262 (9.8) 0.252 (9.81)
TNE average tracheid radial diameter	−42.2*	146.33	*P. aspleniifolius*	1657–2012	0	1,2	0.430 0.355	0.261 (9.76) 0.249 (9.70)
TNE average density	−42.2*	146.33	*P. aspleniifolius*	1657–2012	0	1,2	−0.425 −0.294	−0.194 (7.26) −0.137 (5.33)
Mickey Creek ring width	−41.48	146.42	*A. cupressoides*	1277–2009	1	1	0.294	0.141 (5.27)
Lake Mackenzie ring width	−41.36	146.33	*A. cupressoides*	1344–2008	1	1	0.282	0.122 (4.56)
Mt Field ring width	−42.4	146.33	*A. cupressoides*	1207–2008	1	1,2	0.380 0.326	0.205 (7.67) 0.213 (8.29)
Cradle Mt ring width	−41.4	145.57	*A. selaginoides*	386–2008	1	1	0.273	0.049 (1.83)
Southwest CTP ring width	−42.00*	146.33	*P. aspleniifolius*	1525–2012	1	1,2	0.356 0.338	0.094 (3.52) 0.107 (4.17)
Butters average microfibril angle	−42.09	145.31	*L. franklinii*	1770–2009	0	1,2	0.349 0.328	0.149 (5.57) 0.211 (8.22)
Butters ring average tracheid radial diameter	−42.09	145.31	*L. franklinii*	1770–2009	0	1,2	0.373 0.311	0.159 (5.95) 0.171 (6.67)
Butters ring average density	−42.09	145.31	*L. franklinii*	1770–2009	1	1,2	−0.339 −0.388	−0.134 (5.01) −0.210 (8.18)

[a]A "1" in the Recon column indicates streamflow reconstruction, whereas a "2" indicates the inflow reconstruction. * indicates approximate location as samples were sourced from multiple sites close to one another. The Corr column shows correlations between DJ streamflow (inflow) and predictors used in the reconstruction. The beta column reports beta weights for the initial reconstruction model based on all predictors (nest 1). The figure in brackets next to the beta weights is a percentage and provides an indication of the influence of the predictor on the final chronology. The top figure in each cell in the Corr and beta columns refers to the streamflow reconstruction while the bottom number refers to the inflow reconstruction.

order to extend the reconstruction farther back in time. The individual reconstructions are also rescaled to recover lost variance due to regression in the calibration period. This avoids artificial variability in the nested reconstruction related to differences in R^2. Uncertainty around the nested estimates is typically larger for the longer reconstructions with fewer predictors, but this is explicitly considered in the overall reconstruction uncertainties.

The 50 prewhitened potential tree ring predictors (25 chronologies—nonlagged and lagged 1 year) for inclusion in the model were screened using a two-tail test for significant correlation ($p < 0.1$) with the prewhitened streamflow index (Burbury inflow). Lagged relationships were also tested because previous work has found that the prior season's climate is significantly related to ring widths in many cases [*Buckley et al*., 1997; *Allen et al*., 2001, 2011]. Only those predictors significantly correlated (Pearson correlations, $p < 0.1$) with streamflow (Burbury inflow) were included in subsequent stages of reconstruction development (16 streamflow; 12 inflow). All chronologies passing this stage are listed in Table 2 and their locations are shown in Figure 1. Additionally, their monthly correlation functions shown in supporting information Figure S1 clearly show that strongest correlations between selected chronologies and streamflow generally occur in December–January. All selected chronologies are within 100 km of the Lake Burbury impoundment, and this emphasis on local predictors is consistent with the high regional specificity of precipitation patterns in Tasmania (Figure 1). Eleven of the 16 (streamflow) and 10 of the 12 (inflow) predictors were wood properties chronologies rather than ring width chronologies, indicating that these wood properties generally contain significantly stronger moisture-related signals compared to ring widths. The relatively poor moisture signal contained in many of the ring width chronologies is emphasized by the failure of three west coast *Lagarostobos franklinii* chronologies very close to the Burbury impoundment site to be included in the model as predictors (Figure 1). The species mix of selected predictors included *Lagarostrobos franklinii,*

Athrotaxis selaginoides, Athrotaxis cupressoides, and *Phyllocladus aspleniifolius*, although no *Lagarostrobos franklinii* ring width chronologies were included (Table 2). Correlations between DJ streamflow and those ring width chronologies selected as predictors in the model are generally slightly weaker than those between the wood properties chronologies and DJ streamflow, although this is not the case for the inflow reconstruction (Table 2). These correlations of predictors with streamflow (inflow) are best described as moderate, varying between |0.273| (Cradle Mt ring width) and |0.432| (TNE average cell wall thickness). Where a chronology has been used in both reconstructions, correlations between chronologies and each of streamflow and inflow are very similar, the only exception being TNE average density (Table 2). The beta weights shown in Table 2 are the back-transformed regression coefficients for each predictor chronology. The bracketed figures provide an indication of the relative influence of the chronologies and show the beta weight for a particular chronology as a percentage of the sum of the absolute values of the beta weights of all predictor chronologies [*Frank and Esper*, 2005]. In general terms, influence is higher for wood properties and lower for ring width chronologies, although the influence of the Mt Field ring width chronology is relatively strong in both reconstructions (Table 2). Notably, wood properties chronologies from Mickey Creek and TNE in particular have had relatively large influences on the final reconstructions (Table 2). Predictors were only used in the principal component regression (PCR) stage of the analysis for the period over which there were at least four samples making up the chronology. Although many tree ring based reconstructions apply a 0.85 cutoff level of the expressed population signal (EPS) criterion for the portion of a chronology to be used in a reconstruction, this threshold is nothing more than a suggested guide that may be changed based on "the user's subjective evaluation of accuracy needs" [*Wigley et al*., 1984]. With this in mind, we found that portions of chronologies not reaching this EPS level were still valuable for reconstruction purposes here (data not shown). Given the selection of chronologies used as predictors in PCR, the minimum Akaike Information Criterion (AIC) criterion was then used to select the regression model used for reconstruction [see *Cook et al*., 1999], and the maximum entropy bootstrap [*Vinod and Lòpez-de-Lacalle*, 2009] was applied to both the predictors and the streamflow (inflow) series to produce 300 replicates of the reconstruction in order to estimate model uncertainty for each year. This bootstrapping process also enabled nonparametric estimates of uncertainty of the calibration/verification statistics to be calculated [*Cook et al*., 2013]. Prediction intervals providing a measure of the uncertainty associated with individual estimates were also calculated in the manner described by *Cook et al*. [2013]. Prediction intervals are necessarily wider than confidence intervals because there is greater uncertainty associated with an individual estimate than there is with the estimation of the central value. See *Olive* [2007] for details.

Typically, tree ring reconstruction models are calibrated against a subset of the available climate data. Data withheld from this process are then used for verification purposes and a number of statistics used to check model quality in the calibration and verification periods. The longer 1966–2007 period was used for calibration of our streamflow index (inflow) reconstructions. The period 1946–1965 was withheld for verification purposes. Although this verification period is relatively short, it was important to ensure that the range of variability contained in the instrumental record overall could be captured in the calibration period in order to avoid the "no-analogue" problem that can arise, for example, if a model calibration is based solely on a period that contains low flows whereas outside this period, flows were much higher. Two statistics are commonly used to gauge model quality in the calibration period. The simplest and most familiar of these is the coefficient of determination R^2 (CRSQ), a measure of the goodness of fit of the model. It is, however, known to be a poor measure of the goodness of fit if the model is applied to periods outside the calibration period [*Cook et al*., 1999]. The CVRE, or cross-validation reduction of error, calculated using a leave-one out procedure, provides a less biased estimation of calibrated variance compared to R^2. Three statistics are commonly used to assess the credibility of the calibrated model over the verification period. The least rigorous of these is the square of the Pearson correlation R^2 (VRSQ), which is insensitive to changes in mean level between actual and reconstructed values. More rigorous is the reduction of error (RE) statistic that provides a comparison of the sum of squared differences in actual and estimated data with the squared differences between the actual data and its mean. RE ranges between $-\infty$ and 1 and any positive value is considered to indicate some model skill in excess of the calibration period mean of the actual data. The coefficient of efficiency (CE) is the most rigorous of the three statistics used to gauge model skill. Like RE, it ranges from $-\infty$ to 1 but compares squared differences in actual and estimated data with the squared differences in actual data and its mean over the verification period [*Cook et al*., 1999]. A $CE > 0$ indicates a model has greater skill than simply the verification period mean of the actual data.

3. The Reconstructions

Our DJ streamflow and inflow reconstructions are the first verified multicentennial flow reconstructions for the mesic environment of western Tasmania. The only other attempt to reconstruct Tasmanian streamflow using tree rings was hampered by short flow records [*Campbell*, 1982]. The similarity between our two reconstructions (Figures 3c and 3f) is expected given the high degree of similarity between the actual inflow data and the streamflow index (Figure 2). Note that only the period for which point estimates of CE >0 are shown in Figure 3 (see below). Small differences between the reconstructions can be attributed to differences between the streamflow index and inflow series and to the pool of predictors used for the respective reconstructions (Table 2).

3.1. Reconstruction Statistics

The calibration and verification results of our nested streamflow index (inflow) reconstructions are provided in Tables 3 and 4. These statistics are the median estimates based on 300 nested bootstrapped samples. The streamflow reconstruction consists of 11 nested reconstructions and point statistics for each of these nested suites indicate that the streamflow index reconstruction remains valid back to 1530 (Table 3). The inflow reconstruction consists of nine nested reconstructions, and point estimates of RE and CE remain positive back to 1530 (Table 4). While median calibrated variance (e.g., nest 1 0.353 for streamflow and 0.330 for inflow; Tables 3 and 4) is relatively low compared to several other hydrological reconstructions [e.g., *Stahle et al*., 2011; *Cook et al*., 2013; *Pederson et al*., 2013], our reconstructions are nevertheless improvements on the verification period climatology back to 1530 because RE and CE are both >0 (Tables 3 and 4). The nonparametric interval estimates, however (Figure 4), show that RE and CE do not statistically differ from zero ($p < 0.1$) before 1550 for the streamflow reconstruction. Similarly, for the inflow reconstruction, CE and RE are not statistically different from zero before 1530. Notably, 1530 marks the point before which both reconstructions rely exclusively on ring width chronologies. The 90% confidence limits are asymmetrical for the inflow reconstruction RE and CE before 1800 at which time the *Lagarostrobos franklinii* wood properties chronologies drop out (transition to nest 2). In what follows below we primarily focus on the post-1530 reconstruction characteristics.

3.2. The Streamflow and Inflow Reconstructions

According to the reconstructions, with the exception of the Federation Drought ($\sim$1895–1902), the past 200 years has been a period with average or slightly above average flows for DJ. The most severe dry period since 1530 occurred in the late 1600s (Figure 3f). There have been a number of extended periods of below average DJ flows since 1530, as indicated by the smoothed reconstruction (Figure 3): circa 1603–1610, circa1675–1700, circa1720–1740, and the first decade of the twentieth century. The dry period around 1600 was of approximately the same duration and severity as the Federation Drought. In general, the seventeenth century was one of the enhanced variability (Figure 5), and there is a concentration of both low and high flow years in this period (Figures 3c, 3f, and 5). In contrast, there was a relatively low level of variability over the first half of the 20th century, but with noticeably more dry events than wet events (Figure 5). There were also noticeably more wet than dry events in the latter half of the 19th and 20th centuries (Figure 5). Overall, our reconstructions indicate that recent DJ conditions (last two decades) are not unusual and are well within the variability of the past 500 or so years (Figure 3f). According to our reconstructions, DJ conditions of the severity of those occurring from circa 1675 to 1735 are unprecedented since European settlement. Such severe events would likely result in significant socio-economic impacts today, particularly if dry conditions persisted across multiple seasons and/or across large swathes of Australia simultaneously.

4. Other Regional Hydroclimate Records

Our reconstructions contribute toward construction of a paleohydrological history for the broader Australian region. There are a number of historical sources, and streamflow reconstructions, from which information about past hydrological conditions in SEA and beyond can be gleaned. A comparison of these sources and reconstructions reinforces seasonality and geography as important factors requiring explicit consideration in hydroclimatic reconstructions for Australasia.

Mpelasoka et al. [2008] identify five important droughts other than the Federation Drought that have had major impacts on SEA over the past 150 years: 1911–1916, 1918–1920, 1963–1968, 1972–1973, and

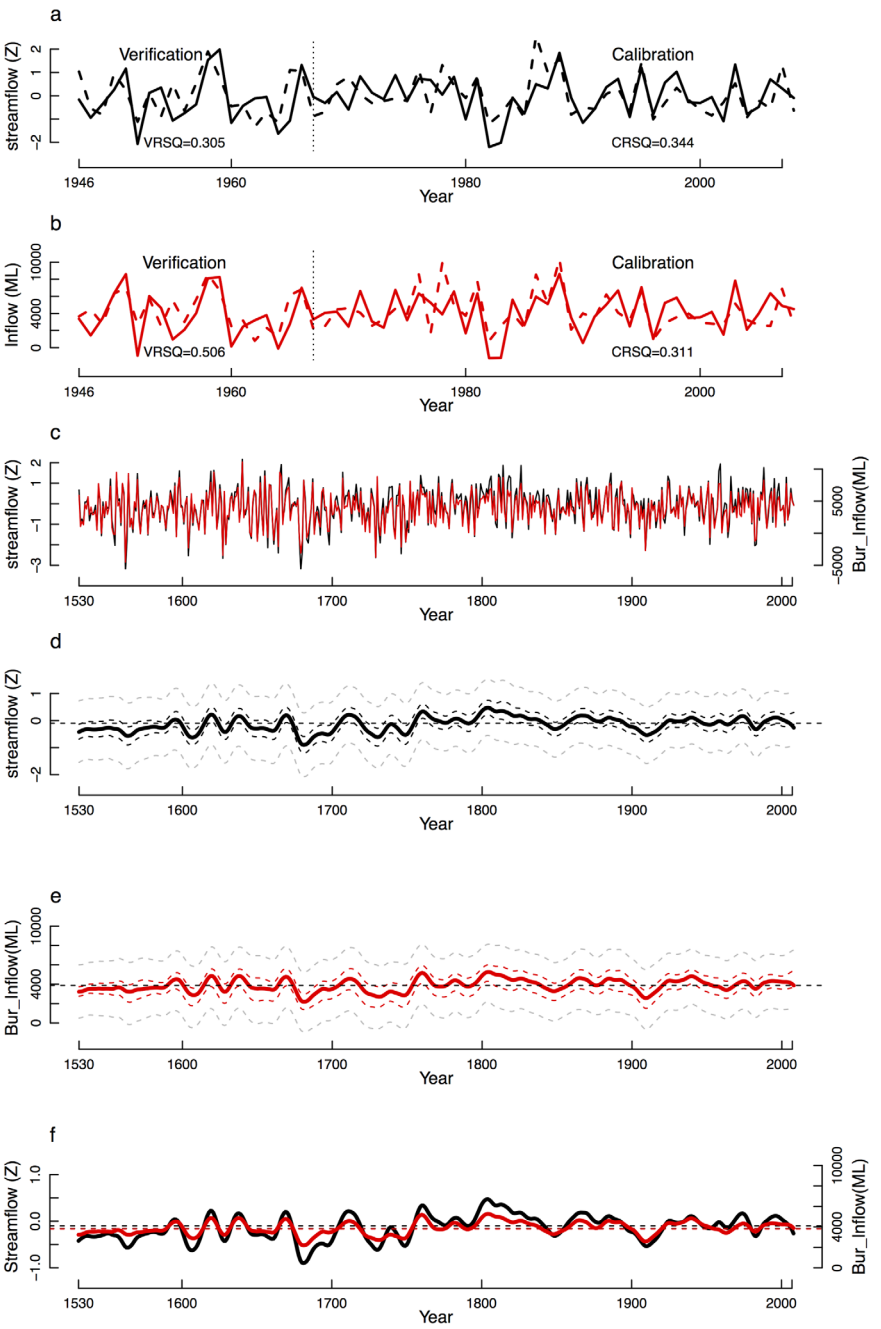

Figure 3. Reconstructed inflows for Lake Burbury and the streamflow index. (a) Actual and reconstructed streamflow over common period. (b) Actual and reconstructed inflows over common period. (c) Streamflow and inflow reconstructions. (d) Reconstructed smoothed (20 year smoothing spline) streamflow with 90% confidence and prediction intervals. (e) Reconstructed smoothed (20 year smoothing spline) streamflow index with 90% confidence and prediction intervals. For Figures 3d and 3e, prediction intervals shown as dashed gray lines, confidence intervals shown as dark dashed lines. (f) Reconstructed smoothed (20 year smoothing spline) Burbury inflows and the smoothed reconstructed streamflow index. Note that streamflow index is displayed as z-score series but inflows are measured in ML.

1982–1983. Our reconstruction identifies years within all but one (1972–1973) of the droughts identified by *Mpelasoka et al*. [2008] as being low flow summers (1911, 1915, 1918, 1963, 1982). Of the three major twentieth century droughts often referred to [*Verdon-Kidd and Kiem*, 2009] (Federation Drought, WWII (∼1937–1945) drought and the Big Dry), our reconstruction clearly captures drought around the turn of the twentieth century but does not as clearly reflect the WWII or the Big Dry droughts. The key to these differences between our reconstruction and these records derived directly from observational data is likely associated with the spatial and seasonal footprints of these droughts. For example, the 1972–1973 drought that broke

Table 3. Calibration/Verification Statistics for the Nested Median Streamflow Index Reconstruction (Figure 3)[a]

Nest	Time Span	No. Crns	CRSQ	CVRE	VRSQ	VRE	VCE
1	1800–2007	16	0.353	0.26	0.218	0.163	0.161
2	1720–2007	13	0.336	0.26	0.218	0.163	0.161
3	1700–2007	12	0.313	0.235	0.243	0.193	0.192
4	1690–2007	10	0.262	0.175	0.32	0.197	0.196
5	1560–2007	7	0.23	0.14	0.195	0.109	0.107
6	1550–2007	6	0.21	0.086	0.201	0.141	0.14
7	1530–2007	5	0.21	0.111	0.109	0.054	0.053
8	1430–2007	4	0.168	0.068	0	−0.11	−0.112
9	1360–2007	3	0.166	0.071	−0.001	−0.129	−0.217
10	1210–2007	2	0.155	0.074	−0.013	−0.17	−0.171
11	386–2007	1	0	−0.002	0	0	0

[a]With the exception of the first and last nests, the start years of each nest are rounded up to the next decade. This ensures there is at least a decade between nests. No. crns refers to the number of chronologies included in each nest. Based on these point estimates, the streamflow index reconstruction remains skillful until 1530 at which point both RE and CE fall below zero. Note the monotonic or almost monotonic declines in values of CRSQ, CVRE, and VRSQ over successive nests. Neither RE nor CE decline in a monotonic manner. See also Figure 4.

in January 1973 in Tasmania had relatively little impact on western Tasmania (CSIRO, www.eoc.csiro.au/awap). The WWII drought did not result in large precipitation deficits over western Tasmania, whereas both the Federation and Big Dry droughts did [*Verdon-Kidd and Kiem*, 2009]. However, an important feature of the rainfall deficits experienced during the Big Dry was that they primarily occurred in the autumn months [*Murphy and Timbal*, 2008; *Post et al*., 2014]. In contrast, rainfall deficits during the Federation Drought principally prevailed for the spring and summer months [*Post et al*., 2014], and it is therefore reasonable to expect them to be reflected in our reconstruction whereas deficits largely confined to other seasons should be less apparent.

A comparison of hydrological reconstructions for eastern Australia further reinforces the importance of geographical and seasonal factors, as shown in Figure 6. Reconstructions shown are: *Hendy et al*.'s [2003] coral luminescence record, a proxy for summer Burdekin River flow in Queensland [see also *Lough*, 2011] (Figure 1; location A); *Vance et al*.'s [2014] reconstruction of the IPO reconstruction based on Law Dome ice records [*Vance et al*., 2014], linked to precipitation in region "B" (Figure 1); the Unified ENSO proxy (UEP) [*McGregor et al*., 2010]; *Gallant and Gergis*'s [2011] reconstruction of Murray-Darling streamflow (Figure 1; region C). Wet and dry periods noted by *McGowan et al*. [2009] in their PDO-based reconstruction of headwater inflows to the Murray River (Figure 1; location C) are also noted. There are clear differences among the reconstructions that are likely related to complex interactions of the broadscale processes generating precipitation over eastern Australia, as well as the seasonal signature of the different reconstructions. For example, an IPO signal is unlikely to be reflected in western Tasmanian summer streamflow because the strongest IPO signal in Tasmanian streamflow records occurs in eastern and northern streams in winter (Allen et al., submitted manuscript). In addition, given that the greater proportion of precipitation in SEA falls in the winter-spring season, annual streamflow reconstructions for SEA [e.g., *McGowan et al*., 2009; *Gallant and Gergis*, 2011] are unlikely to correlate strongly with summer flow reconstructions for western

Table 4. Calibration/Verification Statistics for the Nested Median Inflow Reconstruction (Figure 3)[a]

Nest	Time Span	No. Crns	CRSQ	CVRE	VRSQ	VRE	VCE
1	1800–2007	12	0.33	0.255	0.489	0.434	0.422
2	1720–2007	9	0.304	0.227	0.412	0.322	0.308
3	1700–2007	8	0.311	0.231	0.379	0.276	0.257
4	1690–2007	6	0.257	0.183	0.454	0.316	0.304
5	1560–2007	4	0.235	0.161	0.411	0.278	0.265
6	1550–2007	3	0.208	0.133	0.413	0.303	0.291
7	1530–2007	2	0.212	0.138	0.351	0.244	0.229
9	1207–2007	1	0.174	0.093	0.003	−0.097	−0.116

[a]With the exception of the first and last nests, the start years of each nest are rounded up to the next decade. This ensures there is at least a decade between nests. No. crns refers to the number of chronologies included in each nest. Based on these point estimates, the inflow reconstruction remains skillful until 1530 at which point both RE and CE fall below zero. Note the monotonic or almost monotonic declines in values of CRSQ, CVRE, and VRSQ over successive nests. Neither RE nor CE decline in a monotonic manner. See also Figure 4.

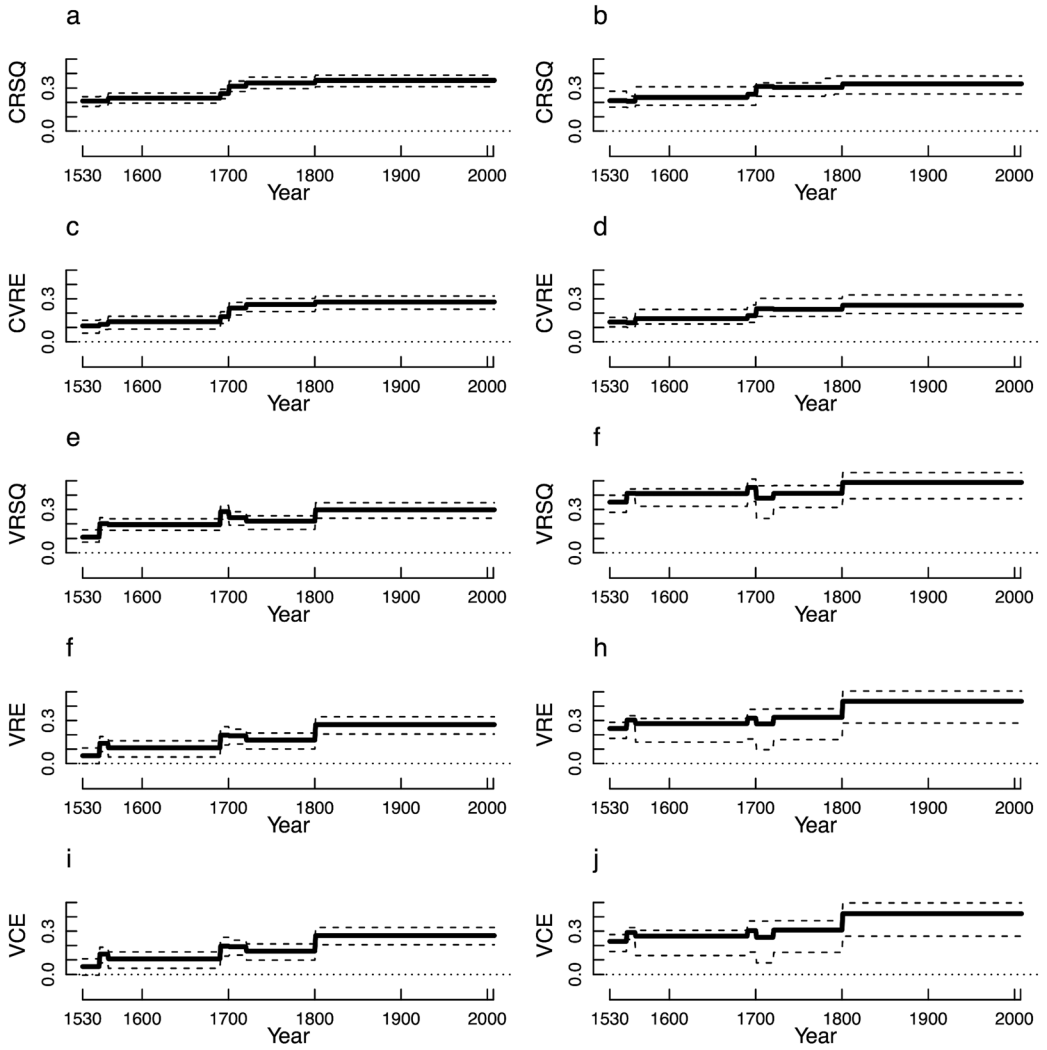

Figure 4. Reconstruction interval statistics over time plotted with bootstrapped 90% confidence intervals. (a, c, e, g, and i) Streamflow index and (b, d, f, h, and j) Burbury inflows. Horizontal dotted line at zero.

Tasmania. Furthermore, the spatial footprint of our DJ reconstructions is limited to western Tasmania (Figures 6d and 6e). Notwithstanding the dominance of differences among reconstructions, some similarities do exist. Our reconstructions, the Havannah coral and Murray River flow reconstruction all capture the Federation drought, and *Gallant and Gergis*'s [2011] record also indicates two periods of high flows in the nineteenth century, also reflected in our record (Figure 6). There are some similarities in the seventeenth century between our reconstructions and *Vance et al.*'s [2014] IPO reconstruction. A strong commonality among the *Gallant and Gergis* [2011], *Hendy et al.* [2003] and our record in the latter part of the twentieth century is also apparent. These intermittent similarities among these records may reflect the relative importance of certain ocean-atmosphere processes at those times.

5. Comparison With Large-Scale Ocean-Atmosphere Processes and Spectral Analysis

We calculated Pearson correlations between our reconstructions and indices of each of the ocean-atmosphere phenomena outlined earlier in section 2.1. Our a priori expectation was that a relatively strong relationship between summer SAM and the DJ streamflow (inflow) reconstructions in western Tasmania would exist, but that relationships with other indices would be weak and nonsignificant. We also used the Multitaper method [*Percival and Walden*, 1993] of spectral analysis ($3 \times 2\pi$ tapers) to look for any significant

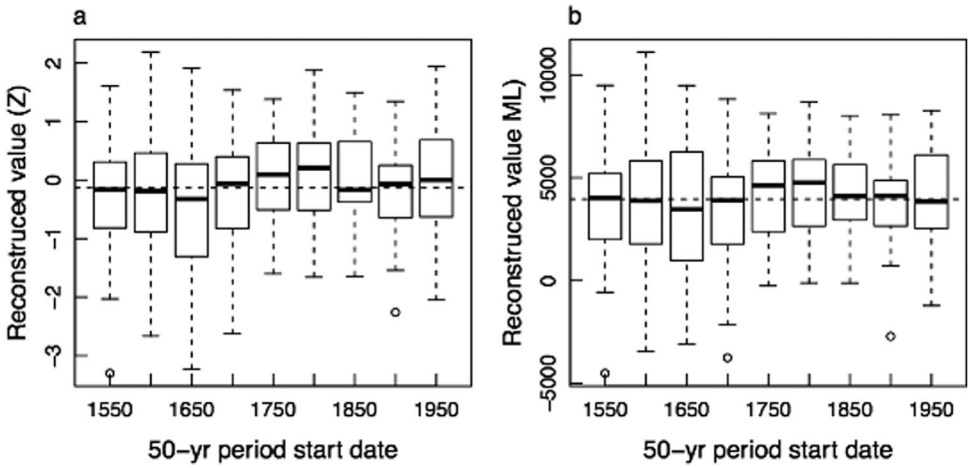

Figure 5. Box and whisker plots calculated for 50 year periods of the streamflow index and Lake Burbury inflow reconstructions. Whiskers show the 10th and 90th percentiles and circles indicate outliers. Horizontal dashed line represents overall median of the reconstruction.

spectral signatures in our reconstructions that may be consistent with known spectral features of these indices.

We found few significant or near significant correlations ($p < 0.05$) between the actual or reconstructed streamflow index (inflow) and indices of broadscale processes (Table 5). Significant correlations with the streamflow index or actual inflows were recorded for the IOD (inflow), Marshall SAM (SAM_M) (actual inflow and streamflow index) and SOI (streamflow index and both reconstructions). That the significant correlation with the IOD occurs in summer, and for only one of the four series, casts some doubt on its validity when the IOD's predominant influence on precipitation is in the north/east of the state and for May to October [*Risbey et al*., 2009]. Significant correlations between the SOI and each of our reconstructions and the streamflow index are consistent with *Grose et al*.'s [2010] observation that the SOI is also an important influence on summer precipitation in western Tasmania (albeit to a lesser extent than SAM). There are strong relationships between the relatively short SAM_M index and both actual inflow and the streamflow index and significant ($p < 0.1$) relationships with the inflow reconstruction. Due to this, and previous work indicating the impact of SAM on summer precipitation in western Tasmania [*Risbey et al*., 2009], we examined relationships between our data and three longer SAM series that are available. The summer (DJF) Fogt index (*Jones et al*. [2009] reconstruction (SAM_J) extends back to 1865 while the *Villalba et al*. [2012] reconstruction (SAM_{VM}) based on tree ring series from South America and New Zealand covers the 1409–2003 period. The Visbeck index (2009; SAM_{VB}) is based on station data. These additional comparisons produced conflicting results. Correlations between the Fogt summer index and our series are highly significant while correlations with *Villalba et al*.'s [2012] summer reconstruction are not ($p < 0.05$; Table 5). Correlations between SAM_{VB} and actual inflow and streamflow are significant ($p < 0.05$) while those with the reconstructions are not. It is possible that the ambiguity of these results is related to the different seasonality of these SAM reconstructions compared to our data and/or that the ambiguity will decrease as additional wood properties chronologies become available and are incorporated into seasonal flow reconstructions. Significant negative correlations between the SOI and each of the streamflow index and its reconstruction, coupled with significant negative relationships between our data and SAM (SAM_M, SAM_J, SAM_{VB}) would be consistent with the positive association between warming in the eastern Pacific (cold-tongue ENSO) and the SAM in the austral summer season [*Lim et al*., 2013; *Vance et al*., 2013].

The dominant periodicity ($p < 0.01$) in both our reconstructions occurs at 3.8 years (Figure 7). Other significant ($p < 0.05$) periodicities in common between the two reconstructions include 2.3, 2.9, 3.1, and 5.6 years. Because spectral analyses were performed only on the 1530–2007 period (477 years), it is not possible to have even two realizations of a 256 year cycle in the period, and hence the significant 256 year periodicity (streamflow) must be treated with great caution. With the exception of the 17.7 year periodicity, all significant ($p < 0.05$) periodicities fall within the ENSO bandwidth, but are also consistent with periodicities found in various SAM indices [*Becagli et al*., 2009; *Yuan and Yonekura*, 2011].

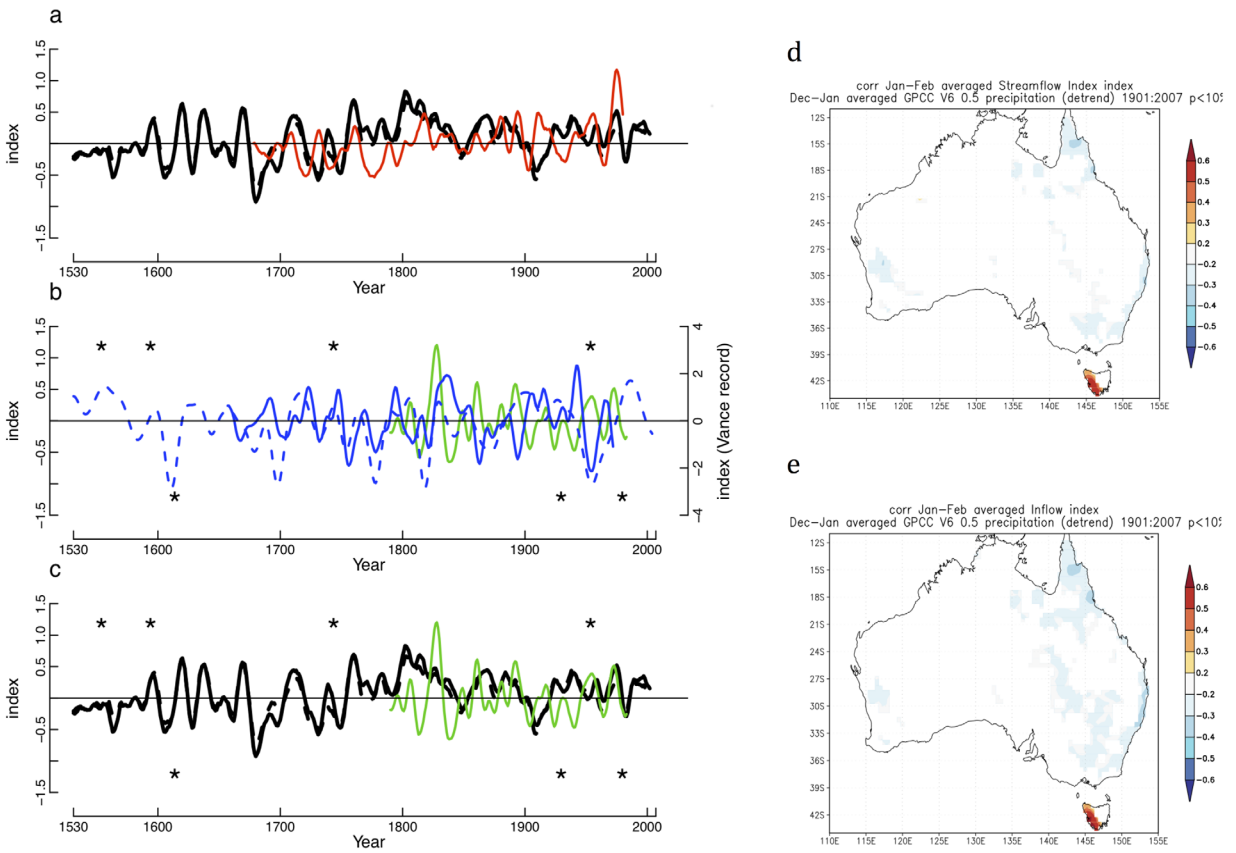

Figure 6. (a–c) Plots of smoothed hydrological reconstructions for eastern Australia, Gaussian filter, n = 13. (a) Summer streamflow and inflow reconstructions for Tasmania and summer Burdekin River flow (Queensland). (b) Summer streamflow and inflow reconstructions for western Tasmania and *Vance et al.*'s [2014] IPO reconstruction, and *McGregor et al.*'s [2010] UEP. (c) Summer streamflow and inflow reconstructions for western Tasmania and *Gallant and Gergis*'s [2011] Murray River flow reconstruction. Black: Tasmanian streamflow and inflow reconstructions; red: *Hendy et al.*'s [2003] Havannah record; blue solid: *Vance et al.*'s [2014] IPO record; blue dashed: *McGregor et al.*'s [2010] UEP. Stars above (below) series indicate wet (dry periods shown in *McGowan et al.*'s [2009]) reconstruction of annual inflows to the headwater catchments of the Murray River. Data sourced from T. Vance, NOAA National Climate Center database (Great Barrier Reef Coral Luminescence Data, contribution Series 2005-032, 350, Unified ENSO Proxy Reconstruction, contribution Series 2010-015) and A. Gallant. (d) Correlation between December and January streamflow reconstruction and GPCC gridded precipitation over southeastern Australia. (e) Correlation between December and January Lake Burbury inflow reconstruction and GPCC gridded precipitation over southeastern Australia. Figures 3d and 3e constructed using the KNMI website (www.climexp.knmi.nl).

Table 5. Correlation Between Streamflow (Inflow) and Main Ocean-Atmosphere Processes Affecting Tasmania[a]

Index	Streamflow Reconstruction	Actual Streamflow	Inflow Reconstruction	Actual Inflow
SOI	−0.26*	−0.26*	−0.29*	−0.23
IOD	−0.16	−0.31*	−0.18	−0.22*
IPO	0.12	0.05	0.15	0.08
BI	0.07	−0.10	0.00	−0.22
STR	0.12	−0.17	0.14	−0.06
SAM_M	−0.18	−0.52**	−0.24	−0.55**
SAM_J	−0.37**	−0.55**	−0.41**	−0.60**
SAM_{VB}	−0.15	−0.37**	−0.19	−0.41**
SAM_{VM}	0.18	−0.11	0.04	−0.13

[a]One asterisk indicates significance at the $p < 0.05$ level, and two asterisks indicate significance at $p < 0.01$. SOI data were sourced from www.bom.gov.au/climate/current/soihtm1.shtml; Marshall's SAM (SAM_M) from http://www.nerc-bas.ac.uk/icd/gjma/sam.html; the dipole index derived from the HADISST data at http://www.jamstec.go.jp/frsgc/research/d1/iod/; Folland's IPO derived from HADSST2 data sourced from http://72.14.235.132/search?q=cache:7_aWJ8652VUJ: www.iges.org/c20c/IPO_v2.doc?interdecadal?pacific?oscillation?data?folland&cd=1&hl=en&ct=clnk&gl=au; and an updated version of *Pook et al.*'s [2006] Blocking Index (BI) at 140° longitude provided by M. Pook (CSIRO). The STRI was provided by Wasyl Drosdowsky (CSIRO) and its derivation is outlined in *Drosdowsky* [2005]. The summer (DJF) Fogt index (SAM_J) is available from http://polarmet.osu.edu/ACD/sam/sam_recon.html). The SAM_{VM} is *Villalba et al.* [2012] reconstruction and was provided by R. Villalba. SAM_{VB} refers to the *Visbeck* [2009] index and data were provided by M. Visbeck. Only concurrent correlations are shown because precipitation in western Tasmania is related to atmospheric anomalies that have little persistence.

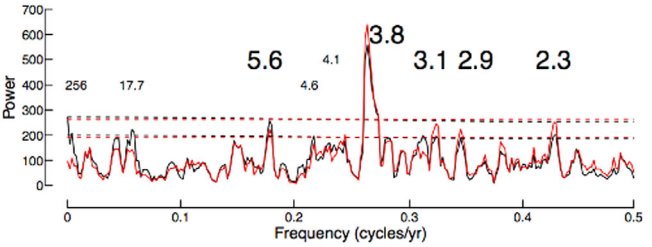

Figure 7. MTM spectra of streamflow and inflow (3 × 2 pi tapers). Solid black line: streamflow; red line: inflow. Significant periodicities ($p < 0.05$) shown. Dashed lines are the 95 and 99% significance levels; black for streamflow, red for inflow. Large figures indicate that the periodicity was significant in both reconstructions. The only significant periodicity in the inflow reconstruction that did not occur in the streamflow reconstruction was at 4.1 years.

6. Discussion and Conclusions

In recent decades, the demand for renewable forms of energy, such as hydroelectricity, has increased [*Clean Energy Council*, 2012]. Coupled with this rising demand is the increasingly urgent need to move toward greater use of renewable energy sources in order to avoid the most serious consequences of anthropogenically induced climate change [*IPCC*, 2014]. As producer of approximately 60% of Australia's renewable hydroenergy, Tasmania's water resources make a pivotal contribution to this goal. However, the ability of Hydro Tasmania to supply more, or even the same amount, of hydroelectricity currently supplied, will depend in large part on future climate. Hydro Tasmania's storage capacity is currently located in western and central Tasmania due to the high annual precipitation received by these areas. Water storages located on Tasmania's Central Plateau are generally at considerably higher elevation than more western storages. This means that power stations fed by the central storages are higher capacity plants than those fed by storages at lower elevation in the west. Projections of decreased precipitation in all seasons for central and northwestern Tasmania [*McIntosh et al*., 2005; *Post et al*., 2009; *Viney et al*., 2009; *Bennett et al*., 2010] and decreased summer streamflow in the west [*Bennett et al*., 2010] intimate that future reliance on summer storage in the west to buffer some of the anticipated shortfall in electricity generation from the central storages may present significant risks. Although it must be remembered that these models are essentially based on 80–100 years worth of observational data, our reconstruction indicates that recent conditions have not been extreme and that there have been both more extended periods of below average flow and much more severe dry periods in the past (Figure 3f). Based on the reconstruction, it would be unwise to rely on the flexibility previously offered by wet December–January periods in the west of the state. This has clear implications for long-term planning and operations management, as well as future infrastructure construction projects. While *Chiew et al*. [2011] have suggested that recent declines in runoff since the 1990s may signal a departure from historical conditions, they may simply represent a transition to drier conditions similar to those that have existed in the past for sustained periods of time.

Although our reconstructions imply that December–January conditions over the past two centuries have generally been wetter than average, they do not provide any information about the hydroclimate of the remaining seasons. Winter precipitation is projected to increase in western Tasmania [*Bennett et al*., 2010], and the bulk of precipitation in western Tasmania falls in the winter-spring season. Projected seasonal changes in the distribution of precipitation [*Chiew et al*., 2014] are likely to have implications for the size and location of future infrastructure development for the generation of hydroelectricity as well as seasonal regulation of impoundment storage levels. There is, therefore, a pressing need for paleohydrological reconstructions of winter-spring hydroclimate to help improve our understanding of its variability over the past 500 years. Ultimately, such long seasonal reconstructions are also likely to provide useful information concerning variability in large-scale ocean-atmosphere processes (e.g., SAM, ENSO, STRI, IOD) that drive the hydroclimate of the region [cf. *Villalba et al*., 2012]. Wood properties chronologies sensitive to winter-spring precipitation (Allen et al., submitted manuscript) are currently being developed from the four long-lived Tasmanian conifers to address this need.

Most other hydrological reconstructions have been developed for regions in which moisture availability is more limiting to growth than in western Tasmania. Therefore, our reconstructions, based heavily on wood properties rather than ring width (Table 2), represent a major step forward, indicating that even for mesic areas like Tasmania it is possible to produce multicentennial verified hydrological reconstructions. As such, they offer much needed long-term information to water managers and planners that is currently unavailable from ring width chronologies. Our work is part of a growing effort to use information other than solely ring widths in tree rings to develop long temperature or hydroclimate reconstructions [*Evans and Schrag*,

2004; *Treydte et al*., 2006; *Brienen et al*., 2012; *Matisons et al*., 2012; *Allen et al*., 2013; *Olana et al*., 2013]. Use of these alternative properties is likely to make available a greater variety of information about past environmental conditions, and from a much greater environmental gradient. Current rapid climatic changes intensify the need to better understand past hydrological conditions in order to incorporate them into quantitative management decision-making frameworks. This need is no less critical in mesic than in arid environments, particularly when large human populations located in these more mesic environments, like SEA, depend on them for domestic and industrial water supplies, agricultural production, recreation, and electricity production.

That we have been able to produce a subannual reconstruction, and preliminary results (Allen et al., submitted manuscript) indicate that reconstructions for other seasonal windows will be possible, is an important breakthrough in a region for which the impacts of the large-scale ocean-atmosphere processes are often simultaneously seasonally and geographically defined [*Murphy and Timbal*, 2008; *Risbey et al*., 2009]. It is all the more significant when decisions in various sectors of the economy must take account of seasonal projections and is similarly important from an ecological management perspective. Our December–January flow reconstructions are therefore, a first step to providing a much more complete climate history for the SEA region.

Acknowledgments

Streamflow and Inflow data are available from Hydro Tasmania and the Department of Primary Industries Parks Water and Environment. Tree ring data will become available via the International Tree-Ring Data Bank (http://www.ncdc.noaa.gov/data-access/paleoclimatology-data/datasets/tree-ring) upon completion of our current project funded by the Australian Research Council and Hydro Tasmania and within 12 months of publication of this paper. The *Lagarostrobos franklinii* wood properties chronologies used in this paper have been contributed to the ITRDB. The reconstructions can be obtained from the corresponding author. We wish to thank Hydro Tasmania and the Department of Primary Industries Parks Water and Environment for provision of the streamflow and inflow data. Mark Willis, Hydro Tasmania, provided descriptive information about catchments. Samples for this study were obtained under permits issued by Forestry Tasmania and Parks and Wildlife Tasmania. Paul Fox-Hughes from the Bureau of Meteorology provided access to information about past hydrological conditions in Tasmania. Ricardo Villalba provided the *Villalba et al*. [2012] SAM reconstruction, Wasyl Drosdowsky provided the STRI, and Martin Visbeck provided the Visbeck SAM index. Greg Lee assisted with production of Figure 1. K.A. and S.N. were supported by an Australian Research Council Linkage Project (LP12020811) cofunded by Hydro Tasmania. P.J.B. was supported by an Australian Research Council Future Fellowship (FT120100751). This paper is also Lamont-Doherty Earth Observatory contribution 7913. We are thankful for the constructive and thoughtful suggestions of three reviewers that have improved this paper.

References

Allen, K. J., E. R. Cook, R. J. Francey, and K. Michael (2001), The climatic response of *Phyllocladus aspleniifolius* (Labill.) Hook. f in Tasmania, *J. Biogeogr.*, *28*, 305–316.

Allen, K. J., J. Ogden, B. M. Buckley, E. R. Cook, and P. J. Baker (2011), The potential to reconstruct broadscale climate indices associated with Australian droughts from Athrotaxis species, Tasmania, *Clim. Dyn.*, *37*, 1799–1821.

Allen, K. J., D. M. Drew, G. M. Downes, R. Evans, E. R. Cook, M. Battaglia, and P. J. Baker (2013), A strong regional temperature signal in low-elevation Huon pine, *J. Quat. Sci.*, *28*, 433–438.

Becagli, S., et al. (2009), Methanesulphonic acid (MSA) stratigraphy from a Talos Dome ice core as a tool in depicting sea ice change and southern atmospheric circulation over the previous 140 years, *Atmos. Environ.*, *43*, 1051–1058.

Bennett, J. C., F. L. N. Ling, B. Graham, M. R. Grose, S. P. Corney, C. J. White, G. K. Holz, D. A. Post, S. M. Gaynor, and N. L. Bindoff (2010), Climate futures for Tasmania: Water and catchments, technical report, Antarct. Clim. and Ecosyst. Coop. Res. Cent., Hobart, Australia.

Brienen, R. J. W., G. Helle, T. L. Pons, J.-L. Guyot, and M. Gloor (2012), Oxygen isotopes in tree rings are a good proxy for Amazon precipitation and El-Niño-Southern Oscillation variability, *Proc. Natl. Acad. Sci. U. S. A.*, *109*, 16,957–16,962.

Buckley, B. M., E. R. Cook, M. J. Peterson, and M. Barbetti (1997), A changing temperature response with elevation for *Lagarostrobos franklinii* in Tasmania, Australia, *Clim. Change*, *36*, 477–498.

Buckley, B. M., K. J. Anchukaitis, D. Penny, R. Fletcher, E. R. Cook, M. Sano, L. C. Nam, A. Wichienkeeo, T. That Minh, and T. Mai Hong (2010), Climate as a contributing factor in the demise of Angkor, Cambodia, *Proc. Natl. Acad. Sci. U. S. A.*, *107*, 6748–6752.

Cai, W., and T. Cowan (2008), Evidence of impacts from rising temperature on inflows to the Murray-Darling basin, *Geophys. Res. Lett.*, *35*, L07701, doi:10.1029/2008GL033390.

Cai, W., T. Cowan, and A. Sullivan (2009), Recent unprecedented skewness towards positive Indian Ocean Dipole occurrences and its impact on Australian rainfall, *Geophys. Res. Lett.*, *36*, L11705, doi:10.1029/2009GL037604.

Campbell, D. (1982), Preliminary estimates of summer streamflow for Tasmania, in *Climate From Tree Rings*, edited by M. K. Hughes et al., pp. 170–177, Cambridge University Press, Cambridge, U. K.

Chen, Z., X. Zhang, M. Cui, M. He, W. Ding, and J. Peng (2012), Tree-ring based precipitation reconstruction for the forest-steppe ecotone in northern Inner Mongolia, China and its linkages to the Pacific Ocean variability, *Global Planet. Change*, *86–87*, 45–46.

Chiew, F. H. S., W. J. Young, W. Cai, and J. Teng (2011), Current drought and future hydroclimate projections in southeast Australia and implications for water resources management, *Stochastic Environ. Res. Risk Assess.*, *25*, 601–612.

Chiew, F. H. S., N. J. Potter, J. Vaze, C. Petheram, L. Zhang, J. Teng, and D. A. Post (2014), Observed hydrologic non-stationarity in far south-easter Australia: Implications for modelling and prediction, *Stochastic Environ. Res. Risk Assess.*, *28*, 3–15.

Clean Energy Council (2012), *Clean Energy Australia Report 2012*. [Available at www.cleannergycouncil.org.au/policy-advocacy/reports.html.]

Cook, E. R., and L. Kariukstis (Eds.) (1990), *Methods of Dendrochronology: Applications in Environmental Science*, Kluwer Acad., Dordrecht, Netherlands.

Cook, E. R., and K. Peters (1997), Calculating unbiased tree-ring indices for the study of climatic and environmental change, *Holocene*, *7*, 361–370.

Cook, E. R., D. M. Meko, D. W. Stahle, and M. K. Cleaveland (1999), Drought reconstruction for the continental United States, *J. Clim.*, *12*, 1145–1162.

Cook, E. R., K. J. Anchukaitis, B. M. Buckley, R. D. D'Arrigo, G. C. Jacoby, and W. E. Wright (2010), Asian monsoon failure and megadrought during the last millennium, *Science*, *328*, 486–489.

Cook, E. R., J. G. Palmer, M. Ahmed, C. A. Woodhouse, P. Fenwick, M. U. Zafar, M. Whab, and N. Khan (2013), Five centuries of Upper Indus flow from tree rings, *J. Hydrol.*, *486*, 366–375.

CSIRO (2008), Water availability in the Murray Darling Basin: A report to the Australian Government from the CSIRO Murray-Darling Basin Sustainable Yields Project, report, 67 pp., Clayton, Australia.

Cullen, L. E., and P. F. Grierson (2009), Multi-decadal scale variability in Autumn-Winter rainfall in south-western Australia since 1655 AD as reconstructed from tree-rings of *Callitris columellaris*, *Clim. Dyn.*, *33*, 433–444.

Drew, D. M., K. J. Allen, G. M. Downes, R. Evans, M. Battaglia, and P. J. Baker (2013), Wood properties in a long-lived conifer reveal strong climate signals where ring width series do not, *Tree Physiol.*, *33*(1), 37–47, doi:10.1093/treephys/tps111.

Drosdowsky, W. (2005), The latitude of the subtropical ridge over eastern Australia: The L index revisited, *Int. J. Climatol.*, *25*, 1291–1299.

Evans, M. N., and D. P. Schrag (2004), A stable isotope-based approach to tropical dendroclimatology, *Geochim. Cosmochim. Acta*, *68*, 3295–3305.
Frank, D., and J. Esper (2005), Temperature reconstructions and comparisons with instrumental data from a tree-ring network for the European Alps, *Int. J. Climatol.*, *25*, 1437–1454.
Friedman, J. H. (1984), A variable span scatterplot smoother, *Tech. Rep. 5*, Standford Univ., Standford, Calif.
Gallant, A. J. E., and J. Gergis (2011), An experimental streamflow reconstruction for the River Murray, Australia, 1783–1988, *Water Resour. Res.*, *47*, W00G04, doi:10.1029/2010WR009832.
Gergis, J., A. Gallant, K. Braganza, D. J. Karoly, K. Allen, L. Cullen, R. D. D'Arrigo, I. Goodwin, P. Grierson, and S. McGregor (2011), On the long-term context of the 1997–2009 'Big Dry' in south-eastern Australia: Insights from a 206-year multi-proxy rainfall reconstruction, *Clim. Change*, *111*, 923–944, doi:10.1007/s10584-011-0263-x.
Grose, M. R., I. Barnes-Keoghan, S. P. Corney, J. Bennett, C. J. White, G. K. Holz, S. Gaynor, and N. L. Bindoff (2010), Climate futures for Tasmania: General climate impact, technical report, Antarct. Clim. and Ecosyst. Coop. Res. Cent., Hobart, Australia.
Heinrich, I., and K. Allen (2013), Current issues and recent advances in Australian dendrochronology; where to next?, *Geogr. Res.*, *51*, 180–191.
Hendy, E. J., M. K. Gagan, and J. M. Lough (2003), Chronological control of coral records using luminescent lines and evidence for non-stationary ENSO teleconnections in northeast Australia, *Holocene*, *13*, 187–199.
Hope, P., B. Timbal, and R. Fawcett (2010), Associations between rainfall variability in the southwest and southeast of Australia and their evolution through time, *Int. J. Climatol.*, *30*, 1360–1371.
IPCC (2014), Climate Change 2014: Synthesis Report. Contribution of Working Groups I, II and III to the Fifth Assessment Report of the Intergovernmental Panel on Climate Change, edited by R. K. Pachauri and L. A. Meyer, 151 pp., IPCC, Geneva, Switzerland. [Available at http://www.ipcc.ch/report/ar5/.]
Jones, J. M., R. L. Fogt, M. Widmann, G. J. Marshall, P. D. Jones, and M. Visbeck (2009), Historical SAM variability: Part I: Century—length seasonal reconstructions, *J. Clim.*, *22*, 5319–5345.
Kiem, A. S., and D. C. Verdon-Kidd (2009), Climatic drivers of Victorian streamflow: Is ENSO the dominant influence?, *Aust. J. Water Resour.*, *13*, 17–29.
Lim, E., H. Hendon, and H. Rashid (2013), Seasonal prediction of the Southern Annular Mode due to its association with ENSO, *J. Clim.*, *26*, 8037–8054.
Lough, J. M. (2011), Great Barrier Reef coral luminescence reveals rainfall variability over northeastern Australia since the 17th century, *Palaeoceanography*, *26*, PA2201, doi:10.1029/2010PA002050.
Marshall, M. (2012), Decline and fall: Civilisations toppled by climate, *New Sci.*, *215*, 33–36.
Matisons, R., D. Elferts, and G. Brumelis (2012), Changes in climatic signals of English oak tree-ring width and cross-sectional area of earlywood vessels in Latvia during the period 1900–2009, *For. Ecol. Manage.*, *279*, 34–44.
McGowan, H. A., S. K. Marx, J. Denholm, J. Soderholm, and B. S. Kamber (2009), Reconstructing annual inflows to the headwater catchments of the Murray River, Australia, using the Pacific Decadal Oscillation, *Geophys. Res. Lett.*, *36*, L06707, doi:10.1029/2008GL037049.
McGregor, S., A. Timmerman, and O. Timm (2010), A unified proxy for ENSO and PDO variability since 1650, *Clim. Past*, *6*, 1–17, doi:10.5194/cp-6-1-2010.
McIntosh, P. C., M. J. Pook, and J. McGregor (2005), Study of future and current climate: A scenario for the Tasmanian region (stages 2 & 3) (CSIRO)—A report for Hydro Tasmania, report, CSIRO Mar. and Atmos. Res., Hobart, Australia.
Melvin, T. M., and K. R. Briffa, (2008), A "signal-free" approach to dendroclimatic standardisation, *Dendrochronologia*, *26*, 71–86.
Melvin, T. M., K. R. Briffa, K. Nicolussi, and M. Grabner (2007), Time-varying-response smoothing, *Dendrochronologia*, *25*, 65–69.
Mpelasoka, F., K. Hennessey, R. Jones, and B. Bates (2008), Comparison of suitable drought indices for climate change impacts assessment over Australia towards resource management, *Int. J. Climatol.*, *28*, 1283–1292.
Murphy, B. F., and B. Timbal (2008), A review of recent climate variability and climate change in southeastern Australia, *Int. J. Climatol.*, *28*, 859–879.
Olana, J. M., A. Arzac, A. I. Garcia-Cervigon, G. van Arx, and V. Rozas (2013), New star on the stage: Amount of ray parenchyma in tree rings shows a link to climate, *New Phytol.*, *198*, 468–495.
Olive, D. J. (2007), Prediction intervals for regression models, *Comput. Stat. Data Anal.*, *51*, 3115–3122.
Pederson, N., C. Leland, B. Nachin, A. E. Hessl, A. E. Bell, D. Martin-Benito, T. Saladyga, B. Suran, P. M. Brown, and N. K. Davi (2013), Three centuries of shifting hydrological regimes across the Mongolian breadbasket, *Agric. For. Meteorol.*, *178–179*, 10–20.
Pederson, N., A. E. Hessl, N. Batatarbileg, K. J. Anchukaitis, and N. Di Cosmo (2014), Pluvial, droughts, the Mongol empire and modern Mongolia, *Proc. Natl. Acad. Sci. U. S. A.*, *111*, 4375–4379.
Peel, M. C., F. H. S. Chiew, A. W. Western, and T. A. McMahon (2000), *Extension of Unimpaired Monthly Streamflow Data and Regionalisation of Parameter Values to Estimate Streamflow in Ungauged Catchments, National Land and Water Resources Audit, Theme 1—Water Availability,* 37 pp., Cent. for Environ. Appl. Hydrol., Univ. of Melbourne, Melbourne.
Percival, D. B., and A. T. Walden (1993), *Spectral Analysis for Physical Applications—Multitaper and Conventional Univariate Techniques*, 580 pp., Cambridge Univ. Press, N. Y.
Pook, M. J., P. C. McIntosh, and G. A. Myers (2006), The synoptic decomposition of cool-season rainfall in the southeastern Australian cropping region, *J. Appl. Meteorol. Climatol.*, *45*, 1156–1170.
Post, D. A. (2013), Regionalizing hydrological response under a changing climate, in *Putting Prediction in Ungauged Basins into Practice*, edited by J. W. Pomeroy, C. Spence, and P. H. Whitfield, chap. 9, pp. 141–152, Can. Water Resour. Assoc., Lethbridge, Canada.
Post, D. A., et al. (2009), Production of climate scenarios for Tasmania: A report to the Australian Government from the CSIRO Tasmanian Sustainable Yields Project, report, CSIRO Water for a Healthy Country Flagship, Clayton, Australia. [Available at http://www.csiro.au/partnerships/TasSY.html.]
Post, D. A., B. Timbal, F. H. S. Chiew, H. Hendon, H. Nguyen, and R. Moran (2014), Decrease in southeastern Australian water availability linked to ongoing Hadley cell expansion, *Earth's Future*, *2*, 231–238.
Risbey, J., M. J. Pook, P. C. McIntosh, M. C. Wheeler, and H. H. Hendon (2009), Remote drivers of Australian rainfall, *Mon. Weather Rev.*, *137*, 3233–3253.
Sheppard, P. R., P. E. Tarasov, L. J. Graumlich, K. U. Heussner, M. Wagner, H. Österle, and L. G. Thompson (2004), Annual precipitation since 515 BC reconstructed from living and fossil juniper growth of northeastern Qinghai Province, China, *Clim. Dyn.*, *23*, 869–881.
Stahle, D. W., F. K. Fye, E. R. Cook, and R. D. Griffin (2007), Tree-ring reconstructed mega-droughts over North America since AD 1300, *Clim. Change*, *83*, 133–149.

Stahle, D. W., J. Villanueva Diaz, D. J. Burnette, J. Ceran Paredes, R. R. Heim Jr., F. K. Fye, R. A. Soto, M. D. Therrell, M. K. Cleaveland, and D. K. Stahle (2011), Major Mesoamerican droughts of the past millennium, *Geophys. Res. Lett.*, *38*, L05703, doi:10.1029/2010GL046472.

Taschetto, A. S., and M. H. England (2008), An analysis of late twentieth century trends in Australian rainfall, *Int. J. Climatol.*, *29*, 791–807.

Timbal, B., and W. Drosdowsky (2012), The relationship between the decline of southeastern Australian rainfall and the strengthening of the subtropical ridge, *Int. J. Climatol.*, *33*, 1021–1034.

Timbal, B., and D. A. Jones (2008), Future projections of winter rainfall in southeast Australia using a statistical downscaling technique, *Clim. Change*, *86*, 165–187.

Touchan, R., K. J. Anchukaitis, D. M. Meko, M. Sabir, S. Attalah, and A. Aloui (2011), Spatiotemporal drought variability in northwestern Africa over the last nine centuries, *Clim. Dyn.*, *37*, 237–252.

Treydte, K. S., G. H. Schleser, G. Helle, D. C. Frank, M. Winiger, G. H. Haug, and J. Esper (2006), The twentieth century was the wettest period in northern Pakistan over the past millennium, *Nature*, *440*, 1179–1182.

Ummenhofer, C. C., M. H. England, P. C. McIntosh, G. A. Meyers, M. J. Pook, J. S. Risbey, A. Sen Gupta, and A. Taschetto (2009), What causes Australia's worst droughts?, *Geophys. Res. Lett.*, *36*, L04706, doi:10.1029/2008GL036801.

Urrutia, R. B., A. Lara, R. Villalba, D. A. Christie, C. La Quesne, and A. Cuq (2011), Multicentury tree ring reconstruction of annual streamflow for the Maule River watershed in south central Chile, *Water Resour. Res.*, *47*, WR06527, doi:10.1029/2010WR009562.

Van Dijk, A. I. J. M., H. E. Beck, R. S. Crosbie, R. A. M. Jeu, Y. Y. Liu, G. M. Podger, B. Timbal, and N. Viney (2013), The millennium drought in southeast Australia (2001–2009): Natural and human causes and implications for water resources, ecosystems and society, *Water Resour. Res.*, *49*, 1040–1057, doi:10.1002/wrcr.20123.

Vance, T. R., T. D. van Ommen, M. J. Curran, C. T. Plummer, and A. D. Moy (2013), A millennial proxy record of ENSO and eastern Australian rainfall from the Law Dome ice core, East Antarctica, *J. Clim.*, *26*, 710–725.

Vance, T. R., J. L. Roberts, C. T. Plummer, A. S. Kiem, and T. D. van Ommen (2014), Interdecadal Pacific variability and eastern Australian megadroughts over the last millennium, *Geophys. Res. Lett.*, *42*, 129–137, doi:10.1002/2014GL062447.

Verdon-Kidd, D. C., and A. S. Kiem (2009), Nature and causes of protracted droughts in southeastern Australia: Comparison between the Federation, WWII, and Big Dry droughts, *Geogr. Res. Lett.*, *36*, L22707, doi:10.1029/2009GL041067.

Villalba, R., et al. (2012), Unusual Southern Hemisphere tree growth patterns induced by changes in the Southern Annular Mode, *Nat. Geosci.*, *5*, 793–798.

Viney, N. R., D. A. Post, A. Yang, M. Willis, K. Robinson, J. C. Bennett, F. L. N. Ling, and S. Marvanek (2009), Rainfall-runoff modelling for Tasmania: A report to the Australian Government from CSIRO Tasmania Sustainable Yields Project, 48 pp., CSIRO Water for a Healthy Country Flagship, Clayton, Australia.

Vinod, H. D., and J. Lòpez-de-Lacalle (2009), Maximum entropy bootstrap for time series: The meboot R package, *J. Stat. Software*, *29*, 1–19.

Visbeck, M. (2009), A station-based Southern Annular Mode Index from 1884 to 2005, *J. Clim.*, *22*, 940–950.

Wigley, T. M. L., K. R. Briffa, and P. D. Jones (1984), On the average value of correlated time series, with applications in dendroclimatology and hydrometeorology, *J. Clim. Appl. Meteorol.*, *23*, 201–213.

Wilson, R. J. S., B. H. Luckman, and J. A. Esper (2005), A 500-year dendroclimatic reconstruction of spring/summer precipitation from the lower Bavarian forest region, Germany, *Int. J. Climatol.*, *25*, 611–630.

Yuan, X., and E. Yonekura (2011), Decadal variability in the Southern Hemisphere, *J. Geophys. Res. Atmos.*, *116*, D19115, doi:10.1029/2011JD015673.